Effect of pre-existing damage on delamination growth in repeatedly indented composites

Huo, L.; Kassapoglou, C.; Alderliesten, R. C.

DOI
10.1016/j.matdes.2024.113068

Publication date
2024

Document Version
Final published version

Published in
Materials and Design

Materials & Design 243 (2024) 113068

Contents lists available at ScienceDirect

Materials & Design

journal homepage: www.elsevier.com/locate/matdes

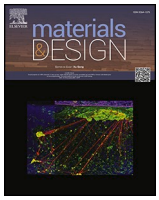

Effect of pre-existing damage on delamination growth in repeatedly indented composites

L. Huo [a,b], C. Kassapoglou [b], R.C. Alderliesten [b,*]

[a] School of Mechanical Engineering, Northwestern Polytechnical University, Xi'an 710072, China
[b] Faculty of Aerospace Engineering, Delft University of Technology, P.O. Box 5058, 2600 GB Delft, The Netherlands

ARTICLE INFO

Keywords:
Polymer-matrix composites
Quasi-static indentation
Delamination growth
Strength degradation

ABSTRACT

Improvements in current design approaches require further studies of the damage interaction effects of composite materials subjected to repeated out-of-plane concentrated loads. To that end, a combined simulation and experimental investigation on composite laminate under repeated indentations is reported. The repeated indentations consist of seven identical peak-force indentations that are separately applied to the centre of the laminate. The results show that delaminations grow in all seven indentations, which can be interpreted as a continuous degradation of the effective delamination growth threshold with each subsequent indentation. More specifically, the second indentation effective delamination growth threshold is 62.4 MPa, which is about 19 % lower compared to the first one (77.2 MPa). Subsequently, the delamination growth threshold degraded approximately linearly with indentation. This effective delamination growth threshold reduction can be associated with the occurrence and evolution of the crack-rich zone preceding the delamination front.

1. Introduction

Fibre-reinforced polymer composite (FRP) laminates are susceptible to out-of-plane loading owing to their low through-thickness strength [1]. Several studies have investigated the damage behaviour of FRP laminates under such loading conditions, which can be classified into quasi-static indentation [2–8], low-velocity impact [9–11], and high-velocity impact [12–15]. The out-of-plane loads involved in these studies are generally applied once at the geometrical centres of the composite targets, and the damage resistances of various composite materials are evaluated or compared. However, such single impacts or indentations may not be sufficient to represent the real-world loading conditions experienced by a composite structure during its entire service life. Foreign objects, such as hailstones, are prone to strike randomly and multiple times on the exposed surfaces of composite structures [16].

A review by Sadighi and Alderliesten [17] showed that extensive studies have been conducted on the damage behaviour of FRP laminates subjected to a more complicated loading condition, namely repeated impacts. This kind of impact loadings considered in previous studies can be roughly divided into two major categories: single impacts at different locations [18,19] and repeated impacts (more than twice) at the same location [20–24]. In the former case, when the two impacts do not occur simultaneously, the damage induced by the first impact can degrade the stiffness and strength properties of the composite targets, which in turn affects the formation of the second impact damage, as described in [25]. The latter is characterised by damage accumulation effects, wherein single impacts may induce minor damages that can accumulate, resulting in significant stiffness and strength property reductions. In this case, the formation of new damage during subsequent impacts is potentially affected by damage-accumulation-induced stiffness and strength property degradation.

For FRP laminates under repeated impacts, researchers usually evaluate the laminate responses in terms of peak impact force versus impact number, peak impact force versus impact energy, impact duration versus impact number, crater diameter or depth versus impact number, projected delamination area versus impact number, residual bending stiffness versus impact number [26]. However, what remains unclear is that how a specific damage mode evolves with subsequent impact load cycles (note that the projected delamination area is usually a superposition of several single delaminations at different ply interfaces, its development cannot reflect how a single delamination grows). According to the authors, the complexity of impact damage, the opaque (CFRP) or translucent (GFRP) natures of the FRP laminates, the transient nature of the impact events, and the unclear one-to-one

* Corresponding author.
E-mail address: R.C.Alderliesten@tudelft.nl (R.C. Alderliesten).

https://doi.org/10.1016/j.matdes.2024.113068
Received 14 March 2024; Received in revised form 15 May 2024; Accepted 3 June 2024
Available online 4 June 2024

Table 1
Unidirectional laminate strengths of M30SC/DT120 (quasi-static loading condition) [31].

Strength	Test method	Test result [MPa]
X_T	ASTM D 3039	3010.0
X_C	ASTM D 6641	1020.0
Y_T	ASTM D 3039	39.0
Y_C	ASTM D 6641	138.0
Z_T*	–	39.0
S_{12}	EN 6031	95.6
S_{13} (S_{23})	EN 2563	77.2

* value is estimated according to Y_T.

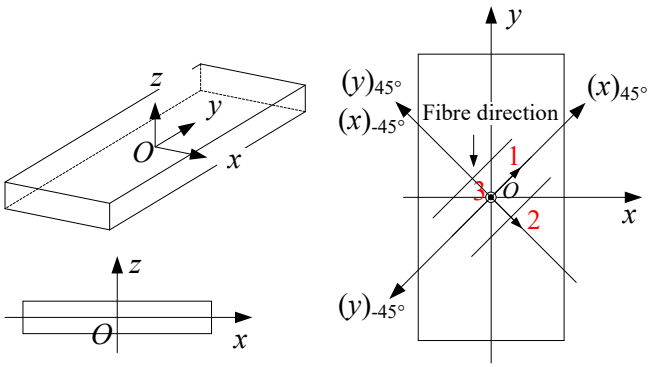

Fig. 1. Cartesian coordinate systems used in this study: global coordinate systems (black *x*-*y*-*z*, $(x)_{-45^\circ}$-$(y)_{-45^\circ}$-*z*) and $(x)_{45^\circ}$-$(y)_{45^\circ}$-*z*) and local coordinate system (red 1-2-3). (For interpretation of the references to colour in this figure legend, the reader is referred to the web version of this article.)

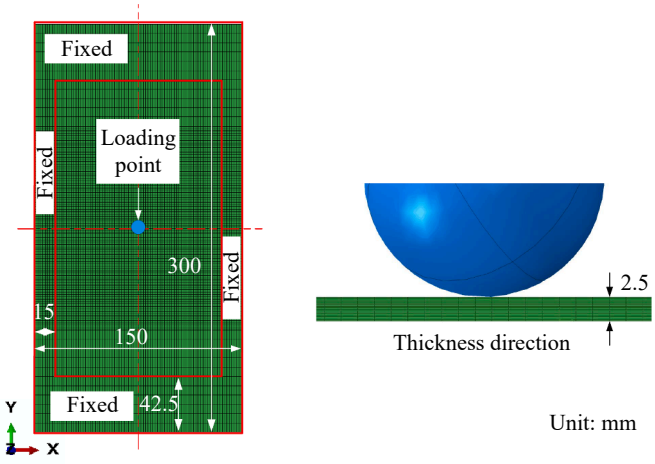

Fig. 2. Details of the FE model used to determine the indentation stress field associated with the single indentation, the layup is $[45/0/-45/90]_{2s}$ [25].

Table 2
Elastic material properties for M30SC/DT120 prepreg.

Young's modulus	$E_{11} = 155$ GPa, $E_{22} = E_{33} = 7.8$ GPa, $G_{12} = G_{13} = 5.5$ GPa, $G_{23} = 2.6$ GPa*
Poisson's ratio	$\nu_{12} = \nu_{13} = 0.27$, $\nu_{23} = 0.5$*

* ν_{23} is estimated, and G_{23} is obtained by assuming that the 2–3 plane is isotropic.

correspondence between the initiation and propagation of specific damage and impact signal features are the main reasons [2,27–30]. These factors together determine the difficulty of observing the

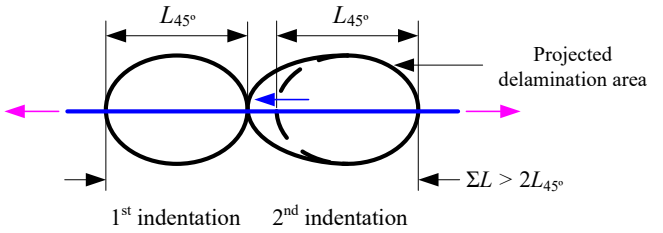

Fig. 3. Illustration of delamination propagation with damage interaction effect in the multiple indented composite laminates.

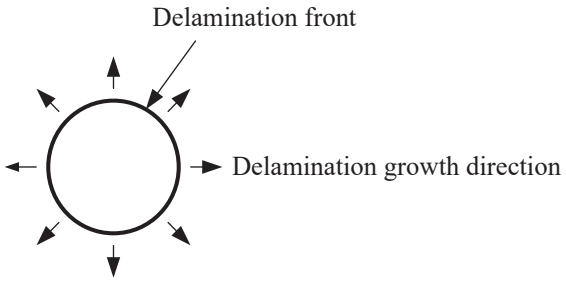

Fig. 4. Illustration of delamination propagations in the composite laminates subjected to repeated indentations at the same point (point-repeated indentation).

initiation and propagation of various impact damage in-situ with current damage detection techniques. To overcome this issue, more directly related parameter(s), such as various damage thresholds, than the impact signal features should be employed to describe damage initiation and propagation, to evaluate the development of a specific repeated impact damage with impact numbers.

The effective damage threshold can be defined as a critical strength value below which a target laminate is unlikely to damage, and is classified into effective matrix crack initiation threshold, effective fibre tensile and compressive failure thresholds, and effective delamination growth threshold [25]. Therefore, the effective damage threshold is a concept used to describe whether a damage initiates or propagates, and how changes in its value with impact number could be used to quantify the effect of pre-existing damage on damage initiation and propagation. As an initial step to addressing how a specific damage mode evolves with loading cycles in a FRP laminate through changes in effective damage threshold, the damage behaviour of delamination growth is considered in this study. The variation in the effective delamination growth thresholds with indentation number is investigated and quantified using an updated delamination failure prediction approach proposed in a previous study of the authors [25]. That method conceptually assumed that the delaminations along the fibre direction grow as long as the out-of-plane shear stress σ_{13} exceeds the effective delamination growth threshold S_{13}. Furthermore, because damage usually results material property degradation, the hypothesis of this work is that the effective delamination threshold is degraded owing to the previously generated damage in composite laminates under repeated impacts. As a result, continuous degradation of the effective threshold with each loading cycle indicates a continuous delamination growth.

Note that the repeated out-of-plane load considered in this study consists of seven consecutive indentations with similar peak forces. The repeated quasi-static indentations were first chosen over repeated impacts primarily because they provide better control over exact loading location than impact, as well as the ability to avoid additional signal noise associated with dynamic vibrations. More specifically, rectangular multidirectional CFRP laminates with four-side clamped boundary conditions were subjected to seven identical indentations exactly at their centre. Ultrasonic C-scanning and cross-sectional damage analysis were

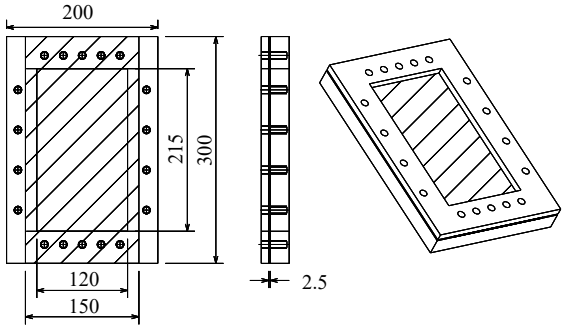

(a) Test clamp. Clamped test specimen is indicated by the hatched area

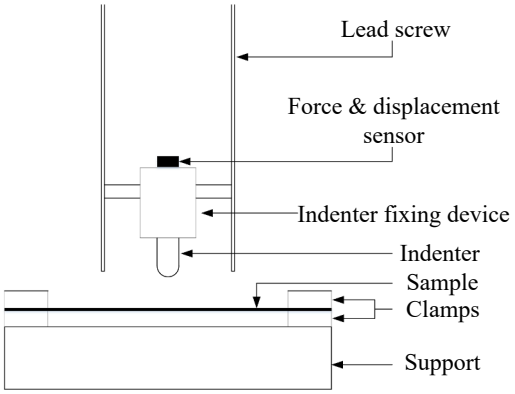

(b) Illustration of the test device

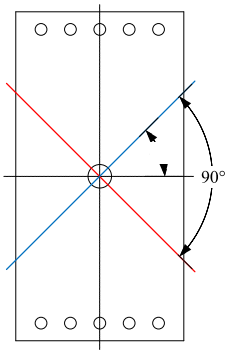

(c) Indentation location

Fig. 5. (a) details of the test clamp, (a) repeated quasi-static indentation test device, and (c) the indentation plan; the adopted global coordinate system is shown in Fig. 1.

Table 3
Test matrix.

Test group	Number of specimens	Predefined indentation force [N]
QSI_01	3	3500
QSI_02	9	4500
QSI_03	3	5500

Note: eight specimens from the test group QSI_02 were used for the microscopic observation (see Fig. 9 and Fig. 10 below). The remaining one specimen and those corresponding to the images demonstrated in Fig. 9(d) and Fig. 10(d) were also used for the ultrasonic C-scan purpose.

used to determine the damage state of the repeatedly indented composite laminates. In addition, to simulate that repeated loading condition, the proposed finite element (FE) model [25] is upgraded with additional indentation cycles accordingly.

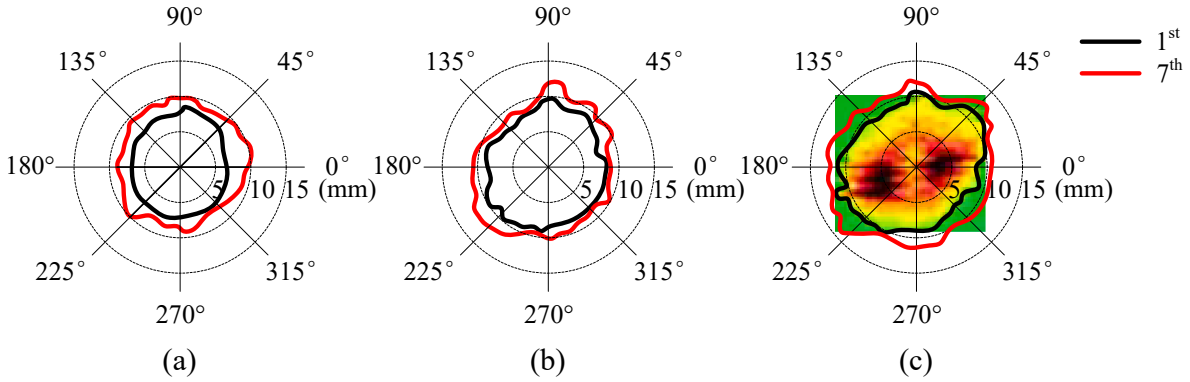

Fig. 6. Comparison of the first and seventh indentation projected delamination areas for the composite laminates under the point-repeated indentations with different peak indentation forces: (a) 3500 N, (b) 4500 N, and (c) 5500 N, the associated global coordinate system is shown in Fig. 1.

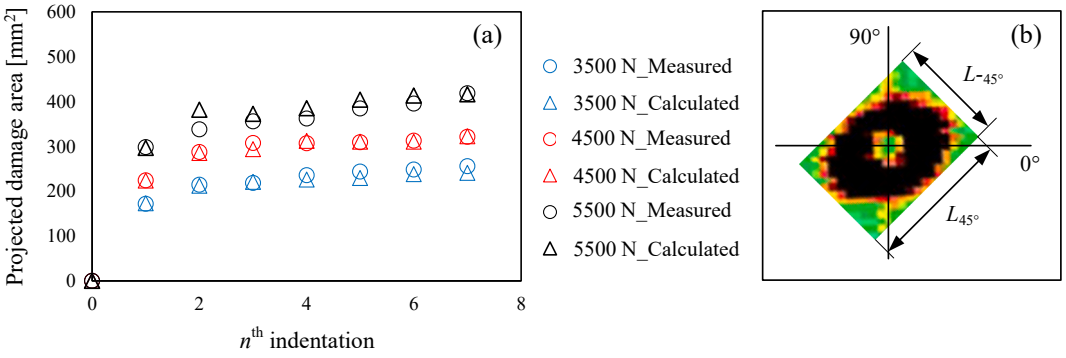

Fig. 7. (a) variations of the experimentally measured projected delamination area and the calculated areas according to the measured L_{45° and L_{-45°, the coefficient of variation is 0.18; (b) definition of the delamination lengths L_{45° and L_{-45°.

2. Basis of the proposed delamination growth prediction method

2.1. Prediction of fibre direction delamination growth under single indentation

The proposed method of the authors [25] for evaluating delamination growth in fibre direction is based on the principle of strength of materials, and the delamination growth criterion associated with this method is as follows:

$$\left(\frac{\sigma_{13}}{S_{13}}\right)^2 = 1 \tag{1}$$

where σ_{13} is the ply interface out-of-plane shear stress and the 1-axis is parallel to the lower ply (i.e., the ply farther away from the indentation site) and the fibre orientation of any two adjacent layers with different fibre directions. S_{13} is the interlaminar shear strength of the unidirectional laminate, which is 77.2 MPa according to the datasheet provided by the manufacturer (Table 1).

The indentation stress profile used to calculate the delamination size was numerically determined using a calibrated FE model, whose dimensions and boundary conditions are presented in Fig. 2. The adopted elastic and strength material properties are summarised in Table 1 and Table 2, respectively. The FE modelling was conducted on an M30SC/DT120 carbon/epoxy composite panel with a layup sequence of $[45/0/-45/90]_{2s}$ and a geometry size of 150 mm × 300 mm × 2.5 mm. The mesh size is 1.74 mm × 1.74 mm × 0.156 mm in the central square region with dimensions of 150 mm × 150 mm × 2.5 mm. The indentation load was applied at the centre of this square region. A mesh sensitivity study was conducted (the mensh sizes considered were 3.48 mm × 3.48 mm × 0.156 mm, 1.74 mm × 1.74 mm × 0.156 mm and 0.87 mm × 0.87 mm × 0.156 mm), which indicated that the FE model with the mesh size of 1.74 mm × 1.74 mm × 0.156 mm had the most acceptable balance between computational time and precision. The boundary condition of this FE model is four-side clamped, i.e., all degrees of freedom (DOF) in the corresponding regions (see Fig. 2, which were marked as 'Fixed') were constrained. Geometric nonlinearity was considered in this model to improve the computational accuracy. The steel hemispherical which with a 25 mm diameter was treated as a rigid body and meshed using R3D4 elements. The contact type between the indenter and composite panel was surface-to-surface, for which the tangential behaviour was described using the penalty method with a 0.3 friction coefficient [32]. Layers of the composite were meshed with C3D8I elements at a thickness of 0.15 mm, in order to precisely calculate the in-plane and out-of-plane stresses using this FE model. Besides, the contact region in the composite laminate was meshed using a higher mesh density compared to other regions. To account for damage-induced stiffness degradation, the model was applied with a published UMAT ABAQUS subroutine [33], which was coded with the Puck failure criterion [34] and the Constant Stress Exposure (CSE) gradual stiffness degradation principle.

The good agreement between the predicted and experimentally measured delamination lengths shown in [25] can well demonstrate the feasibility of the proposed method in predicting the delamination growth along fibre direction. Note that the composite laminate has fifteen ply interfaces in total, and the delamination length in a specific fibre direction is regarded the greatest length among all single delaminations along this direction:

$$L_\Theta = \max\{l_{\Theta 1}, l_{\Theta 2} \cdots l_{\Theta n}\}, \Theta = \{0^\circ, 45^\circ, 90^\circ, -45^\circ\} \tag{2}$$

where $l_{\Theta n}$ is the maximum straight-line length of the single delamination at the n^{th} ply interface (the first ply interface refers to that closest to the indentation point) in the fibre direction Θ. Furthermore, a full discussion of the determination of the delamination length can also be found in [25].

2.2. Prediction of fibre direction delamination growth under multiple indentations

The proposed approach can also be used after adding another indentation to predict delamination growth of composite laminates subjected to two single consecutive indentations [35]. These two indentations with identical peak forces were applied transversely at different distances to composite laminates. As shown in Fig. 3, the second indentation delamination is more likely to propagate in the region between the first and second indentation sites, resulting in a longer delamination length compared to the corresponding single indentation case. This can be regarded as the effective second indentation delamination growth threshold being reduced owing to the pre-existing first indentation damage (matrix cracking and fibre breakage).

To predict the second indentation delamination growth in the region between the first and second indentation sites along the blue line direction, the criterion was calibrated and updated by taking into account the effective delamination threshold degradation with its form as follows:

$$\left(\frac{\sigma_{13}}{\zeta S_{13}}\right)^2 = 1, \zeta = 0.63 \tag{3}$$

where the value of 0.63 provided the best fit with the second indentation experiments.

Combining this updated delamination growth criterion with the out-of-plane shear stress profile determined by the FE model, the eleventh ply interface second delamination growth in the critical cases (i.e., the cases where the delaminations were just connected) of the multiple indented composite laminates under various indentation forces can be

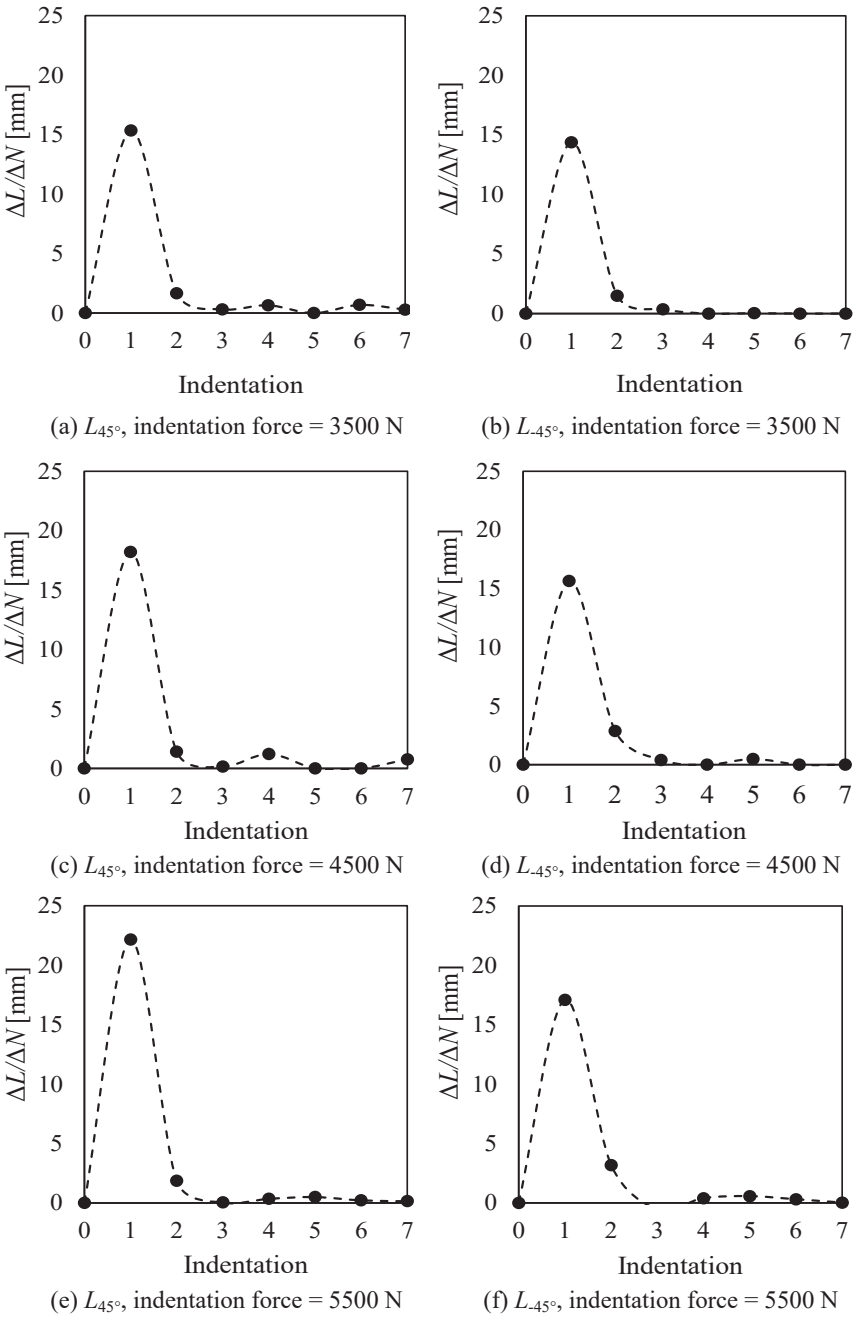

Fig. 8. Delamination growth rates in the 45° and −45° directions for the point-repeatedly indented composite laminates with different indentation forces.

precisely predicted.

3. Concept of point-repeated indentation

As a continuation of the prior studies, the proposed method is extended by adding additional indentation load cycles to quantify the variation in the effective delamination growth threshold with loading cycles for CFRP laminates subjected to the repeated indentations. With this study the effect of pre-existing damage on delamination growth is investigated in how the effective delamination threshold varies with the presence and development of damage. The hypothesis here is that the effective delamination growth threshold is degraded as a result of the damage that formed in the previous indentations, resulting in continued delamination growth in the repeated identical indentations, which can be proven or falsified using the proposed methodology.

Fig. 4 illustrates the case of repeated indentations investigated in this study, which consisted of seven consecutive identical peak-force indentations applied at the centre of the laminates. In this study, the repeated indentation is known as point-repeated indentation. This type of repeated indentation scenario is considered representative of the practical loading condition that composite structures will experience.

For the point-repeated indentation case, as shown in Fig. 4, delaminations formed in previous indentations will continue to grow diametrically outward of the contact region during each subsequent indentation. In this loading condition, along any of the black arrows shown in Fig. 4, delamination formed in subsequent indentation always propagates away from the pre-existing one. In contrast, for the multiple indentation case (Fig. 3), the second indentation delamination grows towards the pre-existing one in the area between two indentation sites. This shows that the considered growth directions of the new

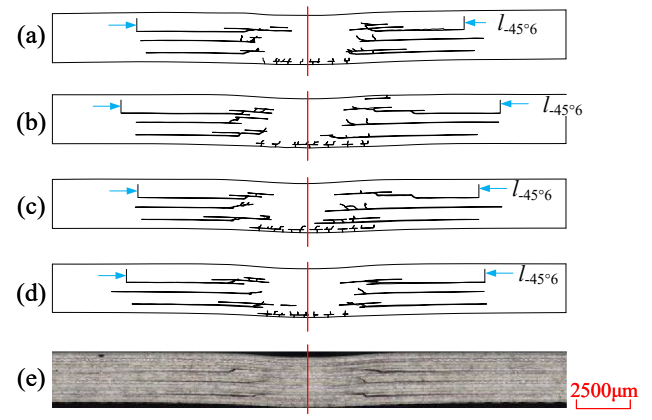

Fig. 9. −45° direction cross-sectional damage morphologies of: (a) after the first indentation; (b) after the third indentation; (c) after the fifth indentation; (d) after seventh indentation; (e) real micrograph of case (d); the indentation force was 4500 N for all cases.

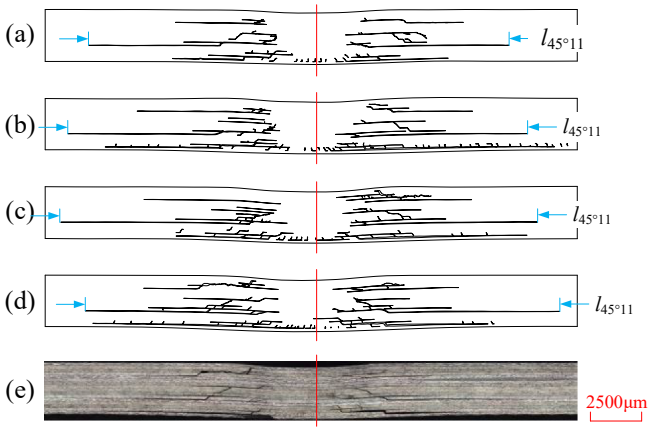

Fig. 10. 45° direction cross-sectional damage morphologies of: (a) after the first indentation; (b) after the third indentation; (c) after the fifth indentation; (d) after the seventh indentation; (e) real micrograph of case (d); the indentation force was 4500 N for all cases.

delaminations respect to the pre-existing delamination of these two cases (Figs. 3 and 4) are opposite. Different relative growth directions could indicate different pre-existing damage influences on the propagation of new delamination. As a result, the point-indentation delamination problem investigated in this study is also primarily concerned with how pre-existing damage influence the formation of new delaminations. It was also investigated using the method proposed in [25] by adding corresponding number of indentations.

4. Experimental details

4.1. Specimen fabrication and test fixture configuration

For consistency with the FE model, the 150 mm × 300 mm × 2.5 mm (nominal dimensions) rectangular CFRP specimens have a quasi-isotropic layup of $[45/0/-45/90]_{2s}$ with a 0° fibre direction parallel to their short edges. These specimens were cut from a large hand-laid-up square CFRP panel with dimensions of 1000 mm × 1000 mm made of M30SC/DT120 carbon/epoxy prepreg supplied by Delta-Tech S.p.A. The panel was placed in an autoclave and cured for 90 min at 120 ℃ and 6 bar. To ensure that the specimens were free of defects (i.e., no defects were found in the indentation area of the composite laminates according to the C-scan results), they were ultrasonically C-scanned prior to the test. Note that the thickness of the raw carbon/epoxy prepreg is 0.25 mm, after curing, the average thickness of each layer of the composite laminate has been reduced to 0.16 mm owing to the flow of the epoxy resin during the curing process. A new test fixture was designed (Fig. 5 (a)) for the repeated quasi-static indentation tests. Under this test fixture, the short edges of the specimen were clamped using bolts, as the long edges were fixed by clamping pressure, and the exposed surfaces of the clamped composite specimens had dimensions of 120 mm × 215 mm.

4.2. Repeated quasi-static indentation testing and damage detection

The repeated quasi-static indentation tests were performed using a Zwick Roell 20 kN servo-hydraulic test machine, which is schematically shown in Fig. 5 (b). The indentation loads were applied vertically on the front surface centre of the specimens through a hemispherical steel indenter with a diameter of 25 mm. All indentations were performed at an identical loading rate of 15 mm/min, and the indentation site was indented severn times. Furthermore, the repeated indentation test was in displacement control. A transducer mounted on the top of the indenter fixture was used to directly record the force–deflection signals, and each indentation started unloading as the predefined indentation forces were reached. The predefined indentation forces were 3500, 4500, and 5500 N. The major test details are listed in Table 3.

The point-repeatedly indented specimens were all ultrasonically C-scanned after each indentation to record the evolution of the projected delamination area with indentation. Note that all the settings were done by the technicians at the Delft Aerospace Structures and Materials Laboratory (DASML), who helped determine the thresholds for the C-scans as well. Subsequently, the specimens with an indentation force of 4500 N were separately indented one, three, five, and seven times and then sectioned along the blue and red lines (Fig. 5(c)) to determine the internal delamination evolution with indentation. The exposed cross-sections were ground using sandpapers with different grain sizes of 82, 46.2, 18, 8, and 5 μm and polished with diamond paste. Finally, all the prepared samples were observed under a Keyence VK-X3000 microscope at 5× and 50× magnification, through which damage

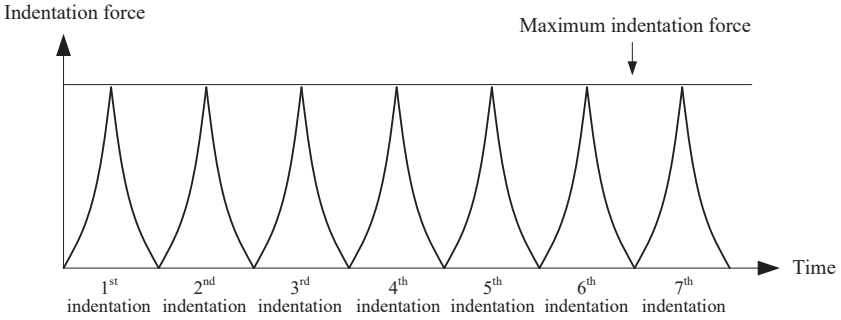

Fig. 11. Illustration of the loading cycles adopted by the FE model used to determine the first to seventh indentation out-of-plane shear stress profiles.

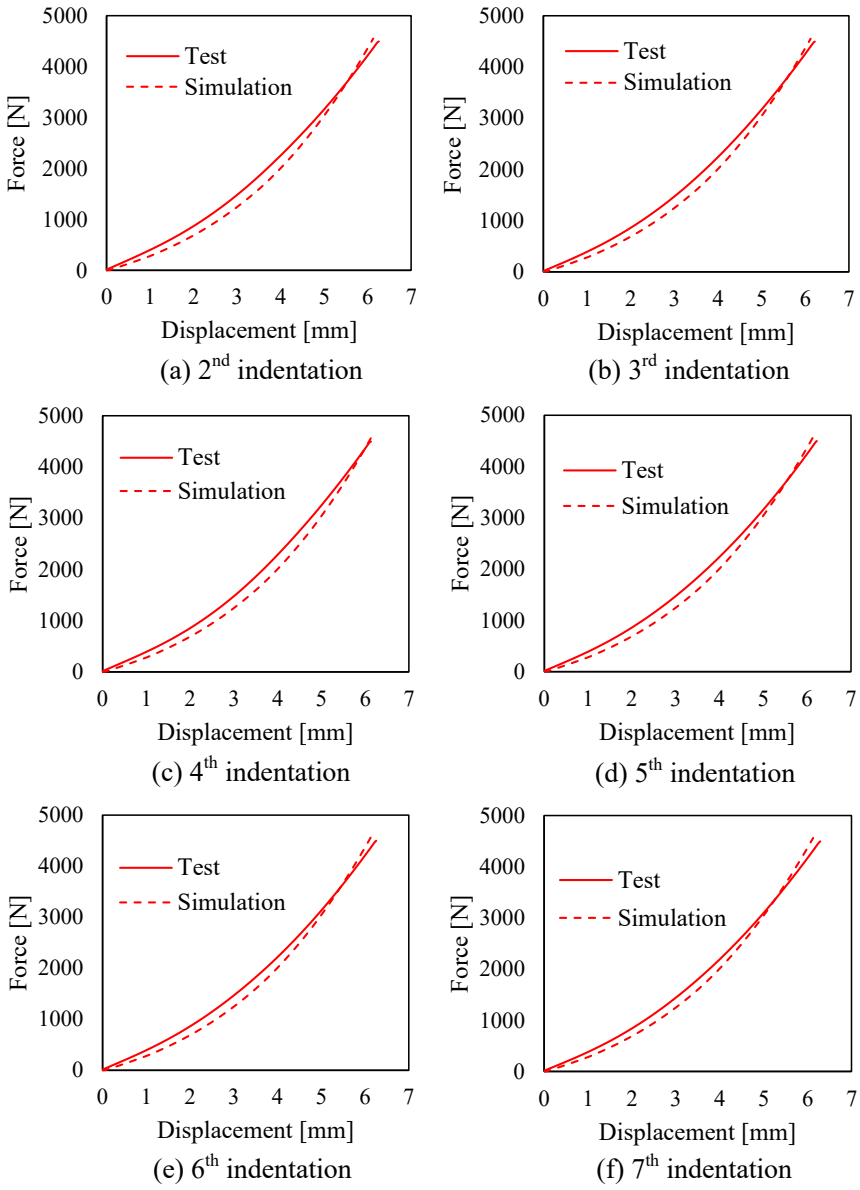

Fig. 12. Comparison of the loading phase of the second to seventh indentation force–displacement curves predicted using the FE model and those obtained from the test, the indentation force is 4500 N for all cases.

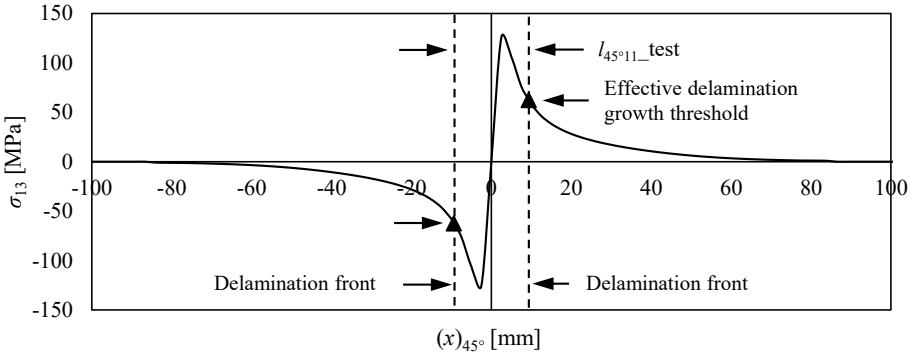

Fig. 13. Determination of the second indentation effective delamination growth threshold at the eleventh ply interface in the 45° direction under the indentation force of 4500 N with the out-of-plane shear stress profiles predicted using the FE model and experimentally measured $l_{45°11}$; the associated coordinate system is shown in Fig. 1.

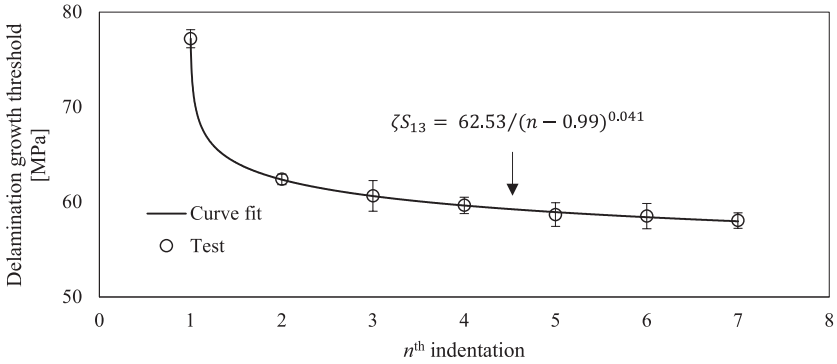

Fig. 14. Variation of the effective delamination growth threshold with indentation in the 45° direction of the point-repeated indentation case, the corresponding indentation force is 4500 N for all indentations.

micrographs were obtained directly. To illustrate the cross-sectional damage morphologies better, these micrographs were post-processed using the AutoCAD 2021 software package.

5. Results and discussion

5.1. Delamination behaviour associated with the point-repeated indentation

5.1.1. Basic features of the indentation delamination

To learn information about the basic propagation feature of the point-repeated indentation delaminations, the specimens were ultrasonically C-scanned after each indentation, and the first and seventh indentation projected delamination areas were compared (Fig. 6). Fig. 6 shows that all of the seventh indentation delaminations had greater projected reas than the first ones, indicating that the delaminations continued to grow after the first indentations, despite the fact that the peak indentation forces are the same for all indentations. This differs with Lee and Zahuta [36] who believed that the first indentation delamination would only grow if the subsequent indentations had rising peak forces. Furthermore, the seventh indentation delaminations did not grow equally in all directions as compared to their first counterparts. For example, the directions with the greatest delamination growth (i.e., the directions along which the maximum difference between the first and seventh indentation delaminations can be measured) are almost 45° (or 225°) for all cases. In contrast, the directions with smallest delamination growth under the indentation forces of 3500 and 5500 N are about 67.5° (or 247.5°), whereas 135° (or the 315°) for the 4500 N indentation case. As a result, all of these delamination areas are irregular ellipses, with the semi-major and semi-minor axes parallel to the 45° and 135° directions (or the 225° and 315° directions), respectively. Note that all specimens were ultrasonically C-scanned using the same equipment with the same setups (the C-scan machine has an accuracy on the order of 1–2 mm for common sizes) and therefore the measurement resolutions for the various cases are comparable.

Owing to that basic oval shape feature, the delamination areas could be expressed by the product of the major and minor axis lengths ($L_{45°}$ and $L_{-45°}$) using the ellipse area formula

$$A = \frac{\pi L_{45°} L_{-45°}}{4} \tag{4}$$

The comparison of the calculated and directly measured areas is shown in Fig. 7. What Fig. 7 shows is that the projected delamination regions were mostly formed during the initial indentations and continued to increase during the next six indentations. Furthermore, the good agreement between the measured and calculated areas revealed that the prediction of the projected delamination area can be simplified to predicting the $L_{45°}$ and $L_{-45°}$. The underlying cause for the continuous increase of the delamination lengths could be the increased stress or reduced effective delamination growth threshold, as suggested by Eq. (1).

To quantify how the delamination area grows with indentation, the delamination growth rate in the 45° and −45° directions is defined as:

$$\frac{\Delta L}{\Delta N} = (L_\Theta)_N - (L_\Theta)_{N-1}, \Theta = \{45^\circ, -45^\circ\}, N \le 7 \tag{5}$$

where L_Θ is the same as defined in Eq. (2), and N refers to the n^{th} indentation, which is not greater than seven in this study. With Eq. (5), the delamination growth rates were calculated and illustrated in Fig. 8. Here, the initial indentation delamination growth rates were correspondingly the largest among all seventh indentations. In contrast, the second growth rates are significantly lower than the first ones, and following growth rates tend to be smaller but more constant throughout the next five indentations.

Because the projected delamination area is a superposition of single delaminations at various ply interfaces, the cross-sectional damage morphologies (Figs. 9 and 10) were used to highlight the correlation between single delaminations and the delamination growth behaviours shown in Fig. 8. The microscope samples belonged to the specimens under the indentation force of 4500 N and were sectioned along the red and blue lines shown in Fig. 5 (c) after their first, third, fifth, and seventh indentations. Figs. 9 and 10 indicate that the sixth and eleventh ply interface delaminations have the biggest sizes in the −45° and 45° directions, respectively. This suggests that the growth characteristics of $L_{-45°}$ and $L_{45°}$ presented in Fig. 8 are essentially associated with the evaluations of $l_{45°6}$ and $l_{45°11}$ for each indentation.

5.1.2. Determination of the shear stress profile and effective delamination growth threshold

To determine the out-of-plane shear stress profiles in the point-repeated indentation case, additional loading cycles were added to update the FE model (Fig. 2). As shown in Fig. 11, the modelling strategy used was to simply numerically indent the composite laminate seven times by setting up seven successive loading cycles with identical peak forces. Through this way, the effects of damage formed in the previous indentations on the shear stress profiles of the subsequent indentations can be properly modelled, making the determination of the second to seventh indentation stress profiles more realistic using the FE model. Note that the FE model was developed to simulate the damage process of the point-repeatedly indented composite laminates; thus, the seven indentations were not a simple repeat of the first indentation in terms of damage formation. This means that, for example, the second indentation should cause additional damage to the first indentation damage.

In this section, the 4500 N indentation delamination growth in the 45° direction was employed to demonstrated how to determine the effective delamination growth threshold using the numerically determined stress profile and experimentally measured delamination length. To that aim, the loading phases of the test and simulation

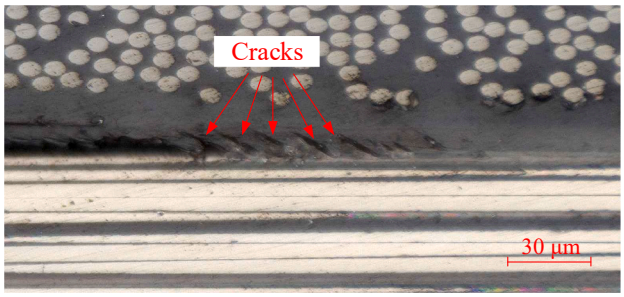

(a) 1st indentation

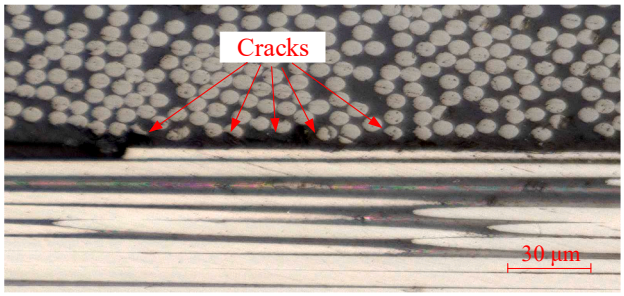

(b) 3rd indentation

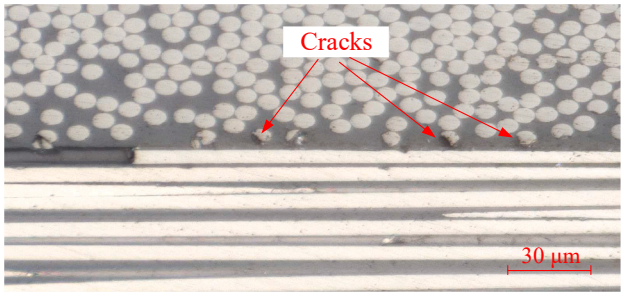

(c) 5th indentation

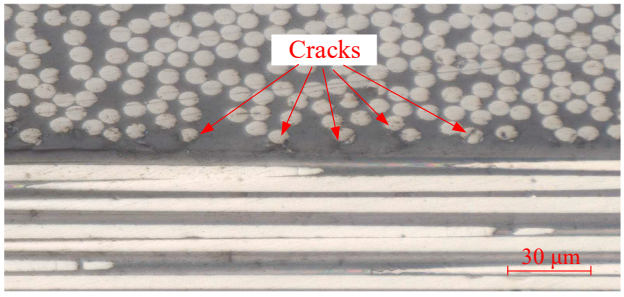

(d) 7th indentation

Fig. 15. Microcracks at the eleventh ply interface delamination front in the 45° direction; the indentation force was 4500 N for all the cases.

force–displacement curves were first compared (Fig. 12).

The acceptable curve matches between the test and simulation results demonstrated that the primary aspects of the global second to seventh indentation stress profiles were captured [25] by that updated FE model. Note that the agreement between the test and simulation force–displacement curves shown in Fig. 12 is not very good (about 20 % disagreement up to 4 mm deflections). However, to facilitate the research, it is assumed that the corresponding shear stress (σ_{13}) distribution can be accurately predicted using this FE model. This assumption was demonstrated to be valid according to the results shown in Fig. 16 and Fig. 17. Besides, more work should be carried out to investigate how the indentation damage affects the global stiffness of the composite

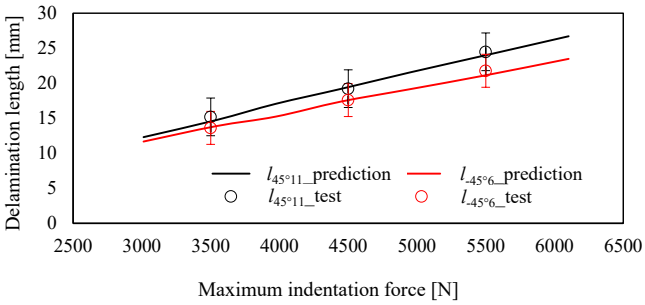

Fig. 16. Comparison of the predicted and experimentally measured $l_{45°11}$ and $l_{45°6}$ of the second indentation of the composite laminates under the indentation forces of 3500, 4500, and 5500 N, respectively; the prediction error in different cases is less than 10 %.

laminate and why the global stiffness of the FE model is smaller than that of the actual composite laminate when assuming a rigid indenter and perfectly clamped boundaries.

The first indentation delamination growth of the point-repeatedly indented composite laminate was not investigated in this study, because the corresponding delamination problem has been addressed in [25]. This explains why the first indentation curves of the test and simulation were not compared in Fig. 12. Following that, the eleventh ply interface shear stress profile was obtained through the FE model. Note that the employed stress profile was exacted from the eleventh ply interface, because the largest delamination size was observed at this interface (Fig. 10). Finally, the detailed steps to determine the effective delamination threshold in the 45° direction, with the second indentation as an example, are shown in Fig. 13.

As shown in Fig. 13, the origin symmetry attribute of the stress profile allows the distance between two symmetrical stress points to be fitted to the measured delamination length (i.e., $l_{45°11}$, and $L_{45°} = l_{45°11}$). The absolute value at the delamination front serves as the effective delamination growth threshold. By following this principle, the average effective delamination growth threshold for each indentation was determined and presented in Fig. 14.

Fig. 14 demonstrates that the average second indentation delamination growth threshold is 62.4 MPa, which is approximately 19 % lower than the first one (77.2 MPa). Subsequently, the delamination growth threshold degraded almost linearly with indentation, and the appropriate criterion for each indentation is as follows:

$$\left(\frac{\sigma_{13}}{\zeta S_{13}}\right)^2_{l_{45°11},4500\ \mathrm{N}} = 1, \zeta = 0.81(n-0.99)^{-0.041}, n = 1,2,3,4,5,6,7. \tag{6}$$

where n refers to the n^{th} indentation. Note that the reduction factor of the second indentation in Eq. (6) differs from that in Eq. (3), which is owing to the considered growth directions of the new delaminations respect to the pre-existing ones of these two cases are opposite (more detailed discussion was provided in Section 3). This means that the reduction factor (zeta) is not a material constant and should be calculated or deduced on a case-by-case basis.

Further, microcracks were observed at the eleventh ply interface delamination front after indentation in the 45° direction. To demonstrate their development, the delamination front photomicrographs of the first, third, fifth, and seventh 4500 N indentation cases were acquired and displayed in Fig. 15. What Fig. 15 highlights is that the crack-rich zone at the delamination front evolves with indentation, and the evolution of the crack-rich zone is considered to be the underlying cause of the effective delamination growth threshold degradation, owing to the fact that the delamination should be more likely to grow in the area with microcracks.

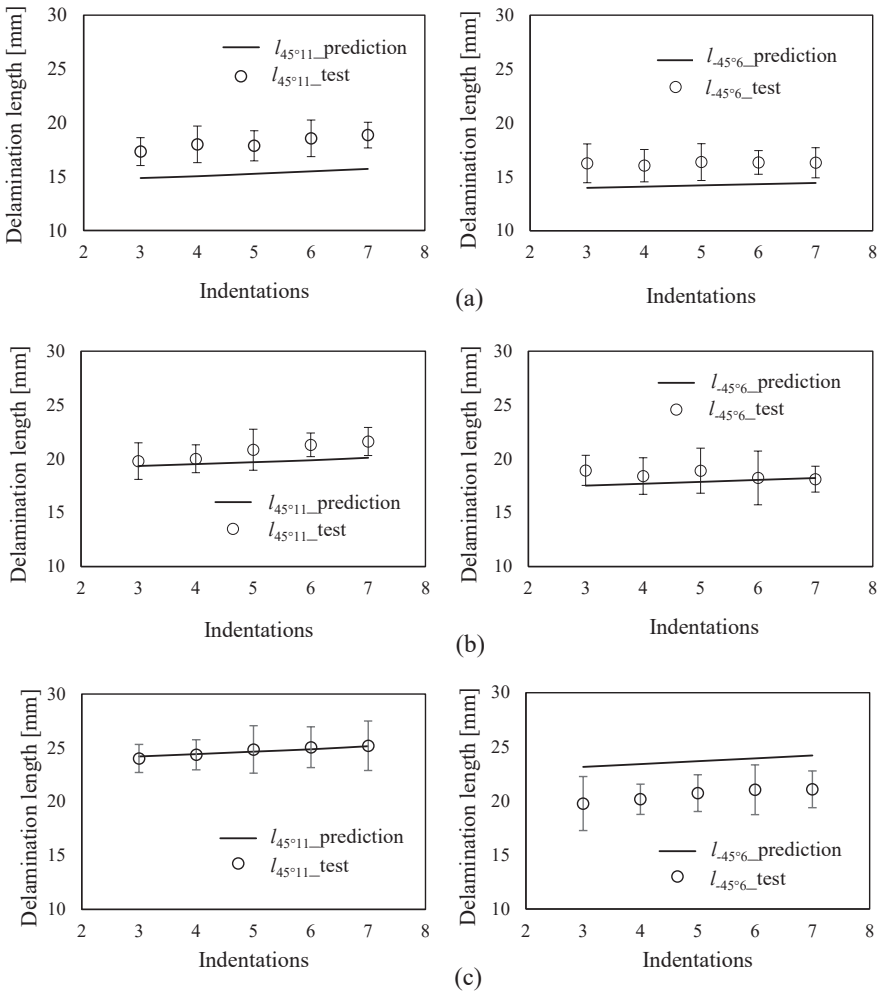

Fig. 17. Comparison of the predicted and experimentally measured $l_{45°11}$ and $l_{-45°6}$ of the third to seventh indentations of the composite laminates under the indentation forces of: (a) 3500 N, (b) 4500 N, and (c) 5500 N; the prediction error in different cases is less than 10 %.

5.2. Indentation force and ply interface independence

To demonstrate the generalisation of the delamination growth criteria in Eq. (6), additional work is required to show their independence from numerous factors, such as indentation force, ply interface, and laminate configuration. In this study, it was considered that those two criteria were independent of the indentation force and that they can be adopted to predict the delamination growth in the −45° direction at the sixth ply interface and the 45° direction at the eleventh ply interface, respectively. As a result, the criterion in Eq. (6) which considered the effective delamination growth reduction should have more general expressions as follows

$$\left(\frac{\sigma_{13}}{\zeta S_{13}}\right)^2_{l_{-45°6},l_{45°11}} = 1, \zeta = 0.81(n-0.99)^{-0.041}, n = 1,2,3,4,5,6,7. \quad (7)$$

Combining the delamination growth criteria shown in Eq. (7) with the stress profiles predicted by the FE model, the $l_{-45°6}$ and $l_{45°11}$ of the second to seventh indentations associated with distinct indentation forces were determined (Figs. 16 and 17). There, the figures demonstrate that the $l_{-45°6}$ and $l_{45°11}$ determined with the criterion and stress profiles closely matched the experimentally measured ones (with prediction errors of 10 % or less). The major error source is the signal noise during the ultrasonic C-scanning, which may change the dimension of the projected delamination area. Nonetheless, the good agreement can well demonstrate the validity of the proposed criteria in describing the sixth ply interface delamination growth in the −45° direction and that at the eleventh ply interface in the 45° direction, as well as the criterion independence from the indentation force. This also indicates that the gradual reduction in the effective delamination growth threshold is the underlying reason for the continued delamination growth (Fig. 7(a)). However, to demonstrate that the criteria are also valid for the delamination growth at any of the interfaces in the lower ply fibre direction [25], adequate damage detection techniques to determine the specific delamination growth at a given ply interface are required.

It is noteworthy that several investigations have been conducted to predict the delamination growth of composites, such as Davies and Robinson in 1992 [37], Suemasu and Majima in 1996 [38], Davies et al. in 2000 [39], Olsson in 2001 [40], Olsson in 2006 [41] and Olsson in 2015 [42]. Davies and Robinson [37] developed a well-established analytical criterion for the growth of a single delamination. Suemasu and Majima [38] derived a more complicated approach for an arbitrary number of delaminations. Later, Olsson et al. (2006) extended Davies & Robinson's simpler method to arrive at the same result. As demonstrated by Davies et al. [39], the analytical delamination criterion may also be combined with FE for arbitrary geometries. Olsson [40] provided arguments as to why delamination growth initiates with a single delamination, and the delamination criterion proposed by Davies and Robinson has been supported by numerous experimental studies. Olsson [42] summarised the analytical criteria for extra failure modes, such as intralaminar shear cracking. On the other hand, the scope of this paper is

currently limited to the delamination growth problem associated with the repeated indentations (i.e., seven identical indentations were applied to the centre of the rectangular composite laminate). Consequently, the proposed delamination growth criterion of this paper took into account the pre-existing damage effects on the propagation of new delamination, which can be used to describe the quasi-static delamination growth under the repeated loading condition. That is, the biggest difference between this delamination growth criterion and those proposed in literature is that the effect of pre-existing damage on the new delamination growth is taken into account.

6. Conclusions

In this study, the delamination growth behaviour of multidirectional composite laminates subjected to repeated out-of-plane indentations was investigated. Repeated indentations were applied to the centre of the composite laminates. The delamination growth of the repeated indentation was studied using the updated delamination growth prediction method. The major conclusion of this study is that, for the point-repeatedly indented composite laminates, delaminations were primarily formed during the first indentation and continued to grow in subsequent indentations. This can be interpreted as a continuous effective delamination growth threshold reduction, which related to the occurrence and development of the crack-rich zone ahead of the delamination front.

It is important to emphasize that damage resistance investigation plays a pivotal role in the design of composite structures. Understanding the damage mechanisms of composite materials is imperative for ensuring their structural integrity and long-term durability. Such investigation significantly contributes to composite structure design by guiding material selection and optimizing design parameters. Notably, the outcomes of this study indicate that repeated out-of-plane loads can exacerbate damage conditions compared to single loading scenarios. Designers must be mindful that damage propagation in composite materials may be influenced by pre-existing damage, and conventional damage resistance tests under single loading conditions may not accurately represent scenarios involving repeated loading.

CRediT authorship contribution statement

L. Huo: Writing – original draft, Visualization, Validation, Methodology, Investigation, Formal analysis, Data curation, Conceptualization. **C. Kassapoglou:** Writing – review & editing, Supervision, Conceptualization. **R.C. Alderliesten:** Writing – review & editing, Supervision, Methodology, Conceptualization.

Declaration of competing interest

The authors declare that they have no known competing financial interests or personal relationships that could have appeared to influence the work reported in this paper.

Data availability

The data related to this paper can be retrieved from the 4TU. ResearchData repository with doi = 10.4121/22265896.v1.

Appendix A. Supplementary data

Supplementary data to this article can be found online at https://doi.org/10.1016/j.matdes.2024.113068.

References

[1] S. Lewis, The use of carbon fibre composites on military aircraft, Compos. Manuf. 5 (2) (1994) 95–103.
[2] A. Wagih, P. Maimí, N. Blanco, J. Costa, A quasi-static indentation test to elucidate the sequence of damage events in low velocity impacts on composite laminates, Compos. A Appl. Sci. Manuf. 82 (2016) 180–189.
[3] V. Dikshit, A.P. Nagalingam, Y.L. Yap, S.L. Sing, W.Y. Yeong, J. Wei, Crack monitoring and failure investigation on inkjet printed sandwich structures under quasi-static indentation test, Mater. Des. 137 (2018) 140–151.
[4] L. Huo, C. Kassapoglou, R. Alderliesten, Influence of neighbouring damage on delamination growth in multiple indented composites, Mater. Des. 227 (2023) 111723.
[5] M.S. Moreno, S.H. Muñoz, Mechanical response of±45° angle-ply CFRP plates under low-velocity impact and quasi-static indentation: Influence of the multidirectional strain state, Compos. Sci. Technol. 194 (2020) 108145.
[6] N.H. Farhood, W.E. Abdul-Lateef, K.F. Sultan, Quasi-static indentation behaviour of carbon-basalt hybrid cylindrical composites, J. Mech. Eng. Res. Dev. 44 (3) (2021) 189–197.
[7] I.I.S. Azhar, A. Jumahat, S. Wam, R. Khiari, Modelling and simulation of quasi-static indentation of kenaf/epoxy composite, Int. Trans. J. Eng., Manage., Appl. Sci. Technol. (2022).
[8] M. Fotouhi, M. Damghani, M.C. Leong, S. Fotouhi, M. Jalalvand, M.R. Wisnom, A comparative study on glass and carbon fibre reinforced laminated composites in scaled quasi-static indentation tests, Compos. Struct. 245 (2020) 112327.
[9] G. Wei, K. Fu, Y. Chen, Crashworthiness and failure analyses of FRP composite tubes under low velocity transverse impact, Sustainability 15 (1) (2022) 56.
[10] N. Aminakbari, M.Z. Kabir, A. Rahai, A. Hosseinnia, Experimental and numerical evaluation of GFRP-reinforced concrete beams under consecutive low-velocity impact loading, Int. J. Civil Eng. 22 (1) (2024) 145–156.
[11] B. Ma, X. Cao, Y. Feng, Y. Song, F. Yang, Y. Li, D. Zhang, Y. Wang, Y. He, A comparative study on the low velocity impact behavior of UD, woven, and hybrid UD/woven FRP composite laminates, Compos. B Eng. 271 (2024) 111133.
[12] V.A. Phadnis, A. Roy, V.V. Silberschmidt, Dynamic damage in FRPs: from low to high velocity, Dynamic Deformation, Damage and Fracture in Composite Materials and Structures, Elsevier 2023, pp. 165-193.
[13] C. Stephen, S.R. Behara, B. Shivamurthy, R. Selvam, S. Kannan, M. Abbadi, Finite element study on the influence of fiber orientation on the high velocity impact behavior of fiber reinforced polymer composites, Int. J. Interact. Des. Manuf. (2022) 1–10.
[14] C.V. Rad, K. Kodagali, J. Roark, D. Revilock, C. Ruggeri, R. Harik, S. Sockalingam, High velocity impact response of hybridized pseudo-woven carbon fiber composite architectures, Compos. B Eng. 203 (2020) 108478.
[15] C.K. Sahoo, G.S. Bhatia, G. Balaganesan, A. Arockiarajan, Post repair high velocity impact behaviour of carbon-glass hybrid composite: Experimental and numerical study, Int. J. Impact Eng. 168 (2022) 104305.
[16] G.J. Appleby-Thomas, P.J. Hazell, G. Dahini, On the response of two commercially-important CFRP structures to multiple ice impacts, Compos. Struct. 93 (10) (2011) 2619–2627.
[17] M. Sadighi, R. Alderliesten, Impact fatigue, multiple and repeated low-velocity impacts on FRP composites: A review, Compos. Struct. 297 (2022) 115962.
[18] B. Liao, P. Wang, J. Zheng, X. Cao, Y. Li, Q. Ma, R. Tao, D. Fang, Effect of double impact positions on the low velocity impact behaviors and damage interference mechanism for composite laminates, Compos. A Appl. Sci. Manuf. 136 (2020) 105964.
[19] J. Zhou, B. Liao, Y. Shi, L. Ning, Y. Zuo, L. Jia, Experimental investigation of the double impact position effect on the mechanical behavior of low-velocity impact in CFRP laminates, Compos. B Eng. 193 (2020) 108020.
[20] B. Liao, J. Zhou, Y. Li, P. Wang, L. Xi, R. Gao, K. Bo, D. Fang, Damage accumulation mechanism of composite laminates subjected to repeated low velocity impacts, Int. J. Mech. Sci. 182 (2020) 105783.
[21] J. Zhou, P. Wen, S. Wang, Numerical investigation on the repeated low-velocity impact behavior of composite laminates, Compos. B Eng. 185 (2020) 107771.
[22] A. Katunin, S. Pawlak, A. Wronkowicz-Katunin, D. Tutajewicz, Damage progression in fibre reinforced polymer composites subjected to low-velocity repeated impact loading, Compos. Struct. 252 (2020) 112735.
[23] B. Sugun, R. Rao, Low-velocity impact characterization of glass, carbon and kevlar composites using repeated drop tests, J. Reinf. Plast. Compos. 23 (15) (2004) 1583–1599.
[24] K. Azouaoui, Z. Azari, G. Pluvinage, Evaluation of impact fatigue damage in glass/epoxy composite laminate, Int. J. Fatigue 32 (2) (2010) 443–452.
[25] L. Huo, C. Kassapoglou, R.C. Alderliesten, A criterion for predicting delamination growth in composite laminates, Mater. Des. 223 (2022) 111160.
[26] L. Huo, R.C. Alderliesten, M. Sadighi, Delamination initiation in fully clamped rectangular CFRP laminates subjected to out-of-plane quasi-static indentation loading, Compos. Struct. 303 (2023) 116316.
[27] L.F.J. Schneider, R.R. Moraes, L.M. Cavalcante, M.A. Sinhoreti, L. Correr-Sobrinho, S. Consani, Cross-link density evaluation through softening tests: effect of ethanol concentration, Dent. Mater. 24 (2) (2008) 199–203.
[28] T.-W. Shyr, Y.-H. Pan, Impact resistance and damage characteristics of composite laminates, Compos. Struct. 62 (2) (2003) 193–203.
[29] A.J. Lesser, A.G. Filippov, Mechanisms governing the damage resistance of laminated composites subjected to low-velocity impacts, Int. J. Damage Mech. 3 (4) (1994) 408–432.
[30] M.P. Cavatorta, D.S. Paolino, Damage variables in impact testing of composite laminates, Composite materials research progress, Nova Science Publishers, Hauppauge, 2008, pp. 241–260.
[31] Delta-tech, DT120-Versatile High Toughness Epoxy Matrix, www.delta-tech.it, 2015.

[32] X. Li, D. Ma, H. Liu, W. Tan, X. Gong, C. Zhang, Y. Li, Assessment of failure criteria and damage evolution methods for composite laminates under low-velocity impact, Compos. Struct. 207 (2019) 727–739.
[33] K. Kodagali, Progressive Failure Analysis of composite Materials using the Puck Failure Criteria, University of South Carolina, 2017. Master thesis.
[34] C.-S. Lee, J.-H. Kim, S.-K. Kim, D.-M. Ryu, J.-M. Lee, Initial and progressive failure analyses for composite laminates using Puck failure criterion and damage-coupled finite element method, Compos. Struct. 121 (2015) 406–419.
[35] L. Huo, R. Alderliesten, C. Kassapoglou, Effect of neighbouring damages on delamination growth in multiple indented composites, to be submitted to Materials & Design (2022).
[36] S.M. Lee, P. Zahuta, Instrumented impact and static indentation of composites, J. Compos. Mater. 25 (2) (1991) 204–222.
[37] G. Davies, P. Robinson, Predicting failure by debonding/delamination, AGARD, Debonding/Delamination of Composites 28 p(SEE N 93-21507 07-24) (1992).
[38] H. Suemasu, O. Majima, Multiple delaminations and their severity in circular axisymmetric plates subjected to transverse loading, J. Compos. Mater. 30 (4) (1996) 441–453.
[39] G. Davies, D. Hitchings, J. Wang, Prediction of threshold impact energy for onset of delamination in quasi-isotropic carbon/epoxy composite laminates under low-velocity impact, Compos. Sci. Technol. 60 (1) (2000) 1–7.
[40] R. Olsson, Analytical prediction of large mass impact damage in composite laminates, Compos. A Appl. Sci. Manuf. 32 (9) (2001) 1207–1215.
[41] R. Olsson, M.V. Donadon, B.G. Falzon, Delamination threshold load for dynamic impact on plates, Int. J. Solids Struct. 43 (10) (2006) 3124–3141.
[42] R. Olsson, Analytical prediction of damage due to large mass impact on thin ply composites, Compos. A Appl. Sci. Manuf. 72 (2015) 184–191.